Letter Vol. 7, No. 4 / April 2020 / Optica 355

optica

Production of 100-TW single attosecond x-ray pulse

Xinrong Xu,[1,2] Yuxue Zhang,[1,4] Hua Zhang,[1,3] Haiyang Lu,[1] Weiming Zhou,[4] Cangtao Zhou,[3] Brendan Dromey,[5] Shaoping Zhu,[6,8] Mathew Zepf,[7] Xiantu He,[1,6] and Bin Qiao[1,*]

[1]Center for Applied Physics and Technology, HEDPS, SKLNPT, and School of Physics, Peking University, Beijing 100871, China
[2]Department of Physics, National University of Defense Technology, Changsha 410073, China
[3]Center for Advanced Material Diagnostic Technology, Shenzhen Technology University, Shenzhen 518118, China
[4]Science and Technology on Plasma Physics Laboratory, Research Center of Laser Fusion, China Academy of Engineering Physics, Mianyang, Sichuan 621900, China
[5]Department of Physics and Astronomy, Queen's University Belfast, Belfast BT7 1NN, UK
[6]Institute of Applied Physics and Computational Mathematics, Beijing 100094, China
[7]Helmholtz Institut Jena, Fröbelstieg 3, 07743 Jena, Germany
[8]e-mail: zhu_shaoping@iapcm.ac.cn
*Corresponding author: bqiao@pku.edu.cn

Received 29 January 2020; revised 21 March 2020; accepted 21 March 2020 (Doc. ID 385147); published 20 April 2020

Attosecond light sources have provided insight into the fastest atomic-scale electronic dynamics. True attosecond-pump–attosecond-probe experiments require a single attosecond pulse at high intensity and large photon energy, a challenge that has yet to be conquered. Here we show 100-TW single attosecond x-ray pulses with unprecedented intensity of 10^{21} W/cm^2 and duration 8.0 as can be produced by intense laser irradiation of a capacitor-nanofoil target composed of two separate nanofoils. In the interaction, a strong electrostatic potential develops between the two foils, which drags electrons out of the second foil and piles them up in vacuum, forming an ultradense relativistic electron nanobunch. This nanobunch reaches both high density and high energy in only half a laser cycle and smears out in others, resulting in coherent synchrotron emission of a single, intense attosecond pulse. Such a pulse enables the capture and control of electron motion at the picometer–attosecond scale.

https://doi.org/10.1364/OPTICA.385147

Forming attosecond pulses—or pulse trains—requires a broad spectral bandwidth with a well-defined phase relationship. Such broad spectra can be generated using the frequency comb formed with high harmonics induced in nonlinear interactions between light and matter [1,2]. High-harmonic generation (HHG) can occur in relativistic plasmas [3–9] with the so-called relativistically oscillating mirror (ROM) mechanism, which can be understood as a periodic Doppler upshifted reflection [6,8,10] of the laser from collective oscillations of the step-like plasma surface. Due to the ability to effectively reflect intense laser fields into harmonic radiation, ROM was previously regarded as a promising route to obtaining bright attosecond pulses when compared to HHG in gases [11–13]. However, the ROM harmonic spectrum has a fast decay scaling of intensity on the harmonic order as $I(n) \propto n^{-8/3}$, which determines that the conversion efficiency from the laser to the attosecond pulse in the large photon energy range is rather low.

Recently, a more efficient radiation mechanism has been identified in which a dense electron nanobunch with a δ-like peak density distribution and relativistic energy is formed outside the target, resulting in coherent synchrotron emission (CSE) [14–16] of XUV/x rays. In CSE, the reflected radiation is proportional to the time derivative of the transverse current density in the nanobunch, instead of a simple phase modulation of the incident laser as ROM. The peak reflected field can exceed that of the incident laser, resulting in a substantial increase in both radiation energy and harmonic orders, where the harmonic spectrum is characterized by a much slower decay scaling as $I(n) \propto n^{-4/3}$ to $n^{-6/5}$.

CSE presents a promising route to extending attosecond radiations at useful brightness levels to the x-ray ($\hbar\omega \sim$ keV) regime. However, to obtain a bright single attosecond x-ray pulse, there are still several key obstacles. First, CSE does not occur in every case of intense laser irradiation on a solid target, since the transition from ROM to CSE regimes is highly sensitive to changes in the plasma density profile, laser amplitude, duration, incident angle, and even the carrier–envelope phase [14,15]. No general description of the required conditions for CSE occurrence has been formulated, and it is hard to discriminate the transition from ROM to CSE where ROM generally dominates. Second, the multi-cycle nature of the drive laser implies that the attosecond radiations must always have come in the form of PHz-repetition-rate trains. Though particle-in-cell (PIC) simulations predict that few-cycle lasers can be used, such laser systems are still under development, and the highest power ($>100-$ TW) lasers currently in operation in laboratories deliver pulse with a duration of several 10s femtoseconds.

In this paper, to overcome the above challenges and achieve a bright single attosecond radiation pulse in a more practical and controlled way, we propose a new robust radiation scheme by using

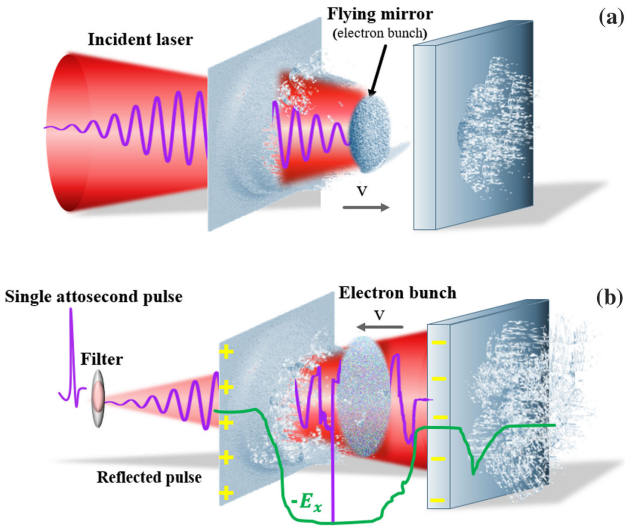

Fig. 1. Schematic for the mechanism of a single attosecond x-ray pulse generation by an intense laser irradiating a capacitor-nanofoil target composed of two separate nanofoils. (a) Electrons of the first nanofoil are blown out at the peak laser cycle, forming a flying relativistic electron mirror, which rapidly impacts the second nanofoil. (b) The second nanofoil acquires significant negative charges, developing a strong electrostatic potential (green) between two foils. This potential drags a large number of electrons out of the second foil and piles them up, forming a dense relativistic electron nanobunch for enhanced CSE of attosecond x-ray pulse.

a capacitor-nanofoil target irradiated normally with intense laser pulses, shown by the schematic in Fig. 1, where two nanofoils are separated with a distance less than laser wavelength λ. The thickness of the first nanofoil satisfies $l_1/\lambda \lesssim (1/2\pi)(n_c/n_1)a_0$ [17], so that all foil electrons are blown out at around the peak laser cycle. Here a_0 is the normalized peak laser amplitude. As shown in Fig. 1(a), the blown-out electrons are rapidly accelerated to relativistic energy, forming a flying dense electron mirror [17], which impacts the second foil quickly. Then, the second foil suddenly acquires significant negative charges, leading to the development of a strong electrostatic potential between two foils [see the green line in Fig. 1(b)]. This strong potential drags a large number of electrons out of the second foil, piling them up in the vacuum gap and forming an ultradense relativistic electron nanobunch [Fig. 1(b)]. CSE occurs when the nanobunch has the maximum compressed electron density n_e, meanwhile moving backwards with the maximum longitudinal velocity v_x, which can be represented by a longitudinal Lorentz factor $\gamma_x = (1 - v_x^2/c^2)^{-1/2}$ at the same laser cycle. The thickness of the second foil is taken to be less than λ, so that for the next laser cycle, the blown-out relativistic electrons return from the rear of the second foil and fill in the gap between two foils, smearing out the electrostatic potential and leading to decompression of the nanobunch. These make CSE substantially less efficient at later cycles, resulting in the production of a single (or few) bright attosecond pulse.

In this novel scheme, achieving CSE is facilitated by a large electrostatic potential developed in the capacitor-nanofoil target, and moreover, the efficient CSE can be restricted to occur only once at around the cycle of the peak laser intensity. More importantly, with the additional contribution of the potential, much denser nanobunches are formed and can be accelerated to much larger momentum $mc\gamma_x$ than possible with a single foil target. This results in much enhanced CSE in the x-ray range and emission of an intense single attosecond x-ray pulse.

The proposed scheme is verified using 1D and 2D PIC simulations with the code "EPOCH" [18]. In 1D simulations, a p-polarized laser with peak intensity $I_0 = 7.7 \times 10^{21}$ W/cm^2 ($a_0 = 60$) and wavelength $\lambda = 800$ nm is used to normally irradiate a capacitor-nanofoil target. The laser pulse has a Gaussian profile in time with FWHM duration $\tau = 4T_0$ ($T_0 = 2\pi c/\lambda$). Both foils of the target are assumed to have a steep density profile of $n_1 = n_2 = 1000n_c$, where $n_c = m\varepsilon_0\omega^2/e^2$ is the critical density. The foil thicknesses are $l_1 = 8$ nm and $l_2 = 100$ nm, where the first nanofoil locates at 20.0λ and the second one at 20.085λ, separated by a distance $d = 60$ nm. The laser starts to interact with the first nanofoil at $t = 20T_0$. The simulation box is 40 λ long with a resolution of $\lambda/100000$. One hundred particles per cell for electrons are taken, and ions are immobile.

In Fig. 2, we see that the main process can be divided into three stages. First, at the early stage, the rising edge of the laser pulse irradiates the first nanofoil, where the intensity is low and the foil remains opaque. The reflected radiation is dominantly due to ROM from the oscillating surface of the first foil, leading to weak, slightly compressed radiation pulse in reflection, as shown with the orange line from $t = 26$ to $27T_0$ in Fig. 2(a).

Second, when the laser reaches peak intensity (from $t = 27$ to $28T_0$) on the first nanofoil, its ponderomotive force exceeds the maximum charge separation field of the foil as $a_0 \gtrsim 2\pi(n_1/n_c)(l_1/\lambda)$, and almost all electrons are blown out towards the second foil. The latter acquires significant negative charges, leading to the development of a strong electrostatic potential between two foils [see the blue line in 2(d)]. As expected, when the laser oscillating ponderomotive force decreases, this strong potential drags a large number of electrons out of the second foil and piles them up, forming an ultradense electron nanobunch with relativistic energy. This can be clearly seen from the electron density distribution of the second foil n_2 by the red line in Figs. 2(d) and 2(e). At $t = 27.57T_0$, the nanobunch is compressed to the maximum density $n_{2,\max} \simeq 2500n_c$ [2(e)] and accelerated to the maximum $\gamma_{x,\max} = 20$ [2(b)]. Meanwhile, the nanobunch interacts with the peak laser field [see the green line in Fig. 2(e)] and reaches its maximum transverse current density gradient. As a result, the reflected laser field is highly compressed, and a remarkable radiation pulse with extreme broad spectral bandwidth and high amplitude is synchronously emitted, seen in the sharp peak of the red line at $t = 27.57T_0$ in Fig. 2(a).

Finally, the blown-out relativistic electrons return from the rear of the second nanofoil and fill in the vacuum. Meanwhile, the electrostatic potential between two nanofoils disappears. Both these lead to smearing out and decompression of the nanobunch [Figs. 2(c) and 2(f)] and eventually the break of CSE in later laser cycles. Figure 2(g) shows that the electrostatic potential developed in the capacitor-nanofoil target contributes not only to the formation of dense electron nanobunches but also a significant enhancement in the acceleration of electrons to a much higher energy than that in a single foil target case.

Figure 2(h) plots the radiation harmonic spectrum [19]. For $\omega < 400\omega_0$, it shows a power law with the exponent $-8/3$ (green). In contrast, for $\omega > 400\omega_0$, it shows a much more slowly decaying power law with the exponent $-4/3$ (red), consistent with that expected from CSE. The harmonics extend up to $\omega = 20000\omega_0$, i.e., photon energy ~30 keV. Such a broadband spectrum leads to

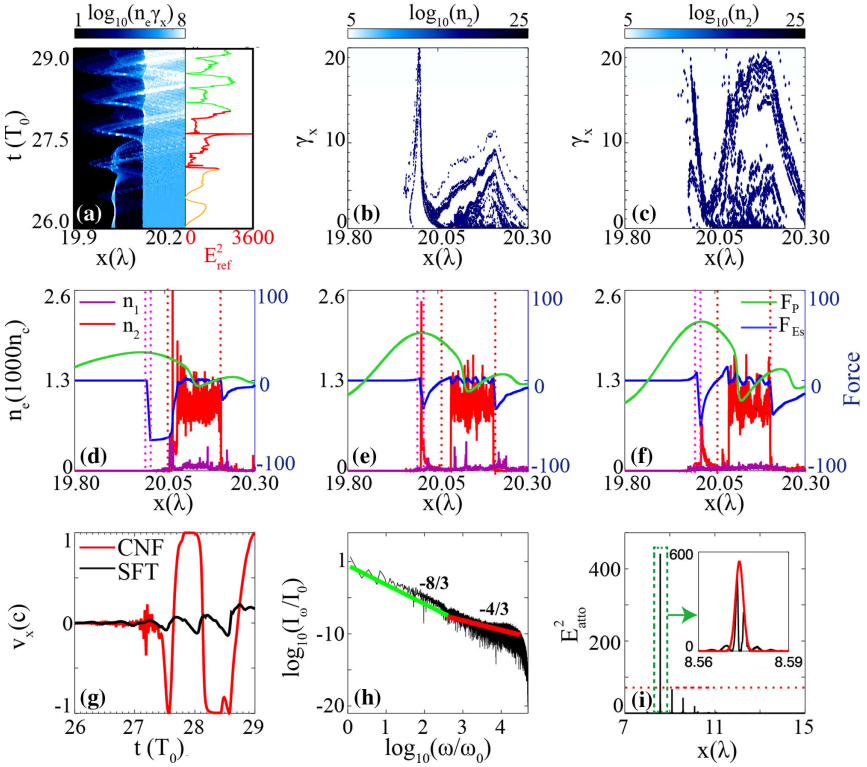

Fig. 2. 1D PIC simulation. (a) Electron longitudinal energy density distribution map $n_e\gamma_x$ evolving with time from $t = 26$ to $29\,T_0$. Square of the corresponding reflected radiation field amplitude $E^2_{\rm ref}$ (orange, red, and green lines) is also plotted. (b), (c) Electron γ_x distributions at $t = 27.57\,T_0$ around the peak of the laser and $28.08\,T_0$ of the next laser cycle, respectively. (d)–(f) Electron density distributions of the first (purple, n_1) and second (red, n_2) foils, electrostatic force (blue), and laser ponderomotive force (green) at $t = 27.48$, 27.57, and $28.08\,T_0$. The initial positions of the two foils are marked with dashed lines. (g) Velocity v_x of one representative electron, for the capacitor-nanofoil target (CNT) and the single foil target (SFT) cases. (h) Harmonic spectrum for radiation in the reflected direction. (i) Obtained radiation pulse amplitude $E^2_{\rm atto}$ versus position x by applying a spectral filter to select $\omega > 100\omega_0$. The inset shows the zoomed single pulse with an envelope fitting (red).

the production of an extremely short radiation pulse. Applying a high-pass spectral filter to select harmonics above $100\omega_0$, an intense single attosecond x-ray pulse with peak intensity $I_{\rm rad} = 9.5 \times 10^{20}$ W/cm^2, duration $\tau_{\rm rad} = 8$ as, and central wavelength $\lambda_{\rm rad} = 2.4$ nm is obtained, [see Fig. 2(i)]. If assuming its transverse radius is 3 μm, its power reaches about 267 TW.

To take into account multi-dimensional effects, 2D PIC simulations are also carried out, where an intense laser pulse with temporally Gaussian and spatially superGaussian (eighth-order) distributions is used and all other parameters are the same as 1D. To save computational resources, the simulation box is composed of $23\lambda \times 10\lambda$ ($\lambda/10000 \times \lambda/1000$). The results are shown in Fig. 3. As clearly seen, a dense electron nanobunch with compressed density $1500n_c$ [Fig. 3(a) and its longitudinal profile in Supplement 1, Fig. S1(a)] and relativistic factor $\gamma_x \approx 6.0$ [Figs. 3(b) and S1(b)] is also formed, which synchronously emits x rays, although the transversely non-planar intensity distribution and much coarser simulation resolution may lead to destructive interference. Figures 3(c) and 3(d) show that a single attosecond x-ray pulse at $I = 2.7 \times 10^{19}$ W/cm^2, $\tau = 14$ as, divergence 2 mrad, and central photon energy ~keV in the normal reflected direction is obtained by the same spectral filter for $\omega > 100\omega_0$.

The proposed scheme is rather robust, which can be tested in experiments soon with high-power lasers, such as petawatt–femtosecond lasers. In experiments, the laser with a high contrast above 10^{10} at picosecond pedestal duration can be achieved by using the plasma mirror [20] or parametric amplification [21]

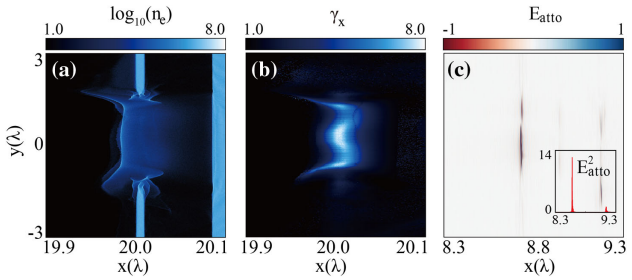

Fig. 3. 2D PIC results. (a), (b) Normalized electron density (n_e/n_c) and longitudinal momentum (γ_x) maps, respectively, at $t = 27.57\,T_0$ around the peak laser intensity. (c) By selecting harmonics above $100\omega_0$, a single attosecond x-ray pulse is produced with $I_{\rm rad} = 2.7 \times 10^{19}$ W/cm^2 ($E^2_{\rm atto} = 12.6$) and $\tau_{\rm rad} = 14$ as (see the inset for its longitudinal profile).

techniques, which can prevent preplasma formation until picoseconds before the main pulse. In order to further prove this, the 1D PIC simulation result with a preplasma scale length of $L = 0.1\lambda$ is shown in Supplement 1, Fig. S2, which clearly implies that a single 13-as pulse is generated successfully. Besides this, the capacitor-nanofoil target, which requires to mount two nanofoils with a distance less than $\lambda/4$ (200 nm), is also makeable with the most advanced target fabrication technologies [22]. Even if the two foils are not parallelly placed, the proposed scheme still works, and a single 30-as pulse with relativistic intensity of 10^{21} W/cm^2 is produced, as shown in Supplement 1, Fig. S3. With the rapid progress

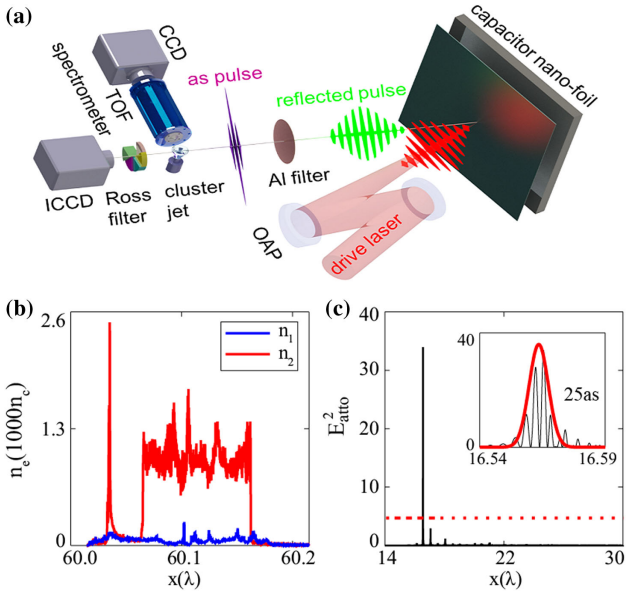

Fig. 4. Demonstrative experimental design for the proposed scheme by using petawatt–femtosecond lasers. (a) Experimental setup. (b), (c) 1D PIC simulation result: (b) compressed ultradense relativistic electron nanobunch of density $2500n_c$ (red line for the electron density of the second foil) is formed, where the blue line is that of the first foil; (c) single attosecond x-ray pulse with intensity $I = 7.3 \times 10^{19}$ W/cm^2 and duration $\tau = 24$ as is obtained with the same filter, where the inset shows the zoomed attosecond pulse with an envelope fitting (red).

of laser and target fabrication technologies, we believe our scheme will be verified very soon.

Here we propose a possible experimental design, shown in Fig. 4(a), in which the attosecond pulse is filtered with a 2.6-μm-thick aluminum foil to reject the laser pulse and 95% x-ray energies below 0.6 keV. The attosecond x-ray pulse can be characterized by measuring its energy spectrum and electric field amplitude. The energy spectrum in the range of 0.6–10 keV usually can be characterized with the x-ray spectrometers, and that of higher 9–50 keV can be measured through the Ross filters. The $-4/3$ power law of the CSE spectrum may be examined by comparing the relative intensities in different energy ranges. Further, the electric field amplitude of the attosecond pulse can be indirectly obtained through applying the pulse for field ionization of hydrogen clusters, where a calculation [23,24] for decoupling of the measured energy spectrum of the Coulomb-exploded protons is required. Detailed consideration of the experimental design is discussed in Supplement 1. To be closer to the current laser conditions, we choose a Gaussian laser with FWHM duration $\tau = 25$ fs, containing 40 laser cycles, where it is generally thought no CSE occurs and no single attosecond pulse can be obtained. The laser intensity is chosen as 7.7×10^{21} W/cm^2 with wavelength of 800 nm. The target parameters are the same as the above 1D simulations. However, the simulation results show that by using the capacitor-nanofoil target, an intense single attosecond x-ray pulse with $I_{rad} = 7 \times 10^{19}$ W/cm^2 and $\tau = 24$ as [Figs. 4(b) and 4(c)] can be produced in our scheme.

In summary, we have proposed a novel, robust scheme to get intense single attosecond pulse in the x-ray regime via the efficient CSE mechanism, which can be achievable by high-power petawatt lasers. By using the capacitor-nanofoil target irradiated with an intense laser, 100-TW single attosecond x-ray pulse with high intensity 10^{21} W/cm^2 and short duration 8.0 can be obtained in the reflected direction. This pulse with many orders of magnitude more powerful than previously reported will permit attosecond probing of processes with much smaller cross-section and pump–probe spectroscopies of a wide range of bound electron exception and relaxation dynamics, which are inaccessible today.

Funding. Science Challenge Project (TZ2018005); NSAF (U1630246); National Key Research and Development Program of China (2016YFA0401100); National Natural Science Foundation of China ((11825502, 11921006); Research Project of NUDT (ZK19-12); Engineering and Physical Sciences Research Council (EP/K022414/1).

Disclosures. The authors declare no conflict of interest.

See Supplement 1 for supporting content.

REFERENCES

1. F. Krausz and M. Ivanov, Rev. Mod. Phys. **81**, 163 (2009).
2. F. Krausz, Phys. Scripta **91**, 063011 (2016).
3. P. Gibbon, Phys. Rev. Lett. **76**, 50 (1996).
4. S. Gordienko, A. Pukhov, O. Shorokhov, and T. Baeva, Phys. Rev. Lett. **93**, 115002 (2004).
5. S. Gordienko, A. Pukhov, O. Shorokhov, and T. Baeva, Phys. Rev. Lett. **94**, 103903 (2005).
6. T. Baeva, S. Gordienko, and A. Pukhov, Phys. Rev. E **74**, 046404 (2006).
7. F. Quéré, C. Thaury, P. Monot, S. Dobosz, P. Martin, J.-P. Geindre, and P. Audebert, Phys. Rev. Lett. **96**, 125004 (2006).
8. B. Dromey, M. Zepf, A. Gopal, K. Lancaster, M. Wei, K. Krushelnick, M. Tatarakis, N. Vakakis, S. Moustaizis, R. Kodama, and M. Tampo, Nat. Phys. **2**, 456 (2006).
9. W. Ma, J. Bin, H. Wang, M. Yeung, C. Kreuzer, M. Streeter, P. Foster, S. Cousens, D. Kiefer, B. Dromey, and X. Q. Yan, Phys. Rev. Lett. **113**, 235002 (2014).
10. U. Teubner and P. Gibbon, Rev. Mod. Phys. **81**, 445 (2009).
11. M. Chini, K. Zhao, and Z. Chang, Nat. Photonics **8**, 178 (2014).
12. J. A. Wheeler, A. Borot, S. Monchocé, H. Vincenti, A. Ricci, A. Malvache, R. Lopez-Martens, and F. Quéré, Nat. Photonics **6**, 829 (2012).
13. T. Popmintchev, M.-C. Chen, P. Arpin, M. M. Murnane, and H. C. Kapteyn, Nat. Photonics **4**, 822 (2010).
14. D. an der Brügge and A. Pukhov, Phys. Plasmas **17**, 033110 (2010).
15. A. Pukhov, D. An Der Brügge, and I. Kostyukov, Plasma Phys. Controlled Fusion **52**, 124039 (2010).
16. B. Dromey, S. Rykovanov, M. Yeung, R. Hörlein, D. Jung, D. Gautier, T. Dzelzainis, D. Kiefer, S. Palaniyppan, R. Shah, and J. Schreiber, Nat. Phys. **8**, 804 (2012).
17. B. Qiao, M. Zepf, M. Borghesi, B. Dromey, and M. Geissler, New J. Phys. **11**, 103042 (2009).
18. T. Arber, K. Bennett, C. Brady, A. Lawrence-Douglas, M. Ramsay, N. Sircombe, P. Gillies, R. Evans, H. Schmitz, A. Bell, and C. P. Ridgers, Plasma Phys. Controlled Fusion **57**, 113001 (2015).
19. R. Lichters, J. Meyer-ter Vehn, and A. Pukhov, Phys. Plasmas **3**, 3425 (1996).
20. B. Dromey, S. Kar, M. Zepf, and P. Foster, Rev. Sci. Instru. **75**, 645 (2004).
21. F. Tavella, A. Marcinkevičius, and F. Krausz, Opt. Express **14**, 12822 (2006).
22. https://www.thorlabs.de.
23. H. Lu, G. Ni, R. Li, and Z. Xu, J. Chem. Phys. **132**, 124303 (2010).
24. H. Lu, J. Liu, C. Wang, W. Wang, Z. Zhou, A. Deng, C. Xia, Y. Xu, X. Lu, Y. Jiang, and Y. X. Leng, Phys. Rev. A **80**, 051201 (2009).